J Opt
https://doi.org/10.1007/s12596-024-02025-3

RESEARCH ARTICLE

Effect of copper addition on lithium zinc borosilicate glass containing terbium oxide

I. Kashif[1] · Sahar Saad Ali[2] · Nourhan. M. Khodeir[2] · Mariam. A. Elhakiem[2] · A. Ratep[2]

Received: 5 April 2024 / Accepted: 29 June 2024

Abstract Terbium lithium zinc borosilicate glass systems incorporating copper ions were prepared using a melt quenching technique. The structural and physical properties of the produced glass samples were investigated using X-ray diffraction (XRD), infrared (FTIR), and optical absorption (UV/Vis/NIR) spectroscopy. The non crystalline behavior of the glasses was confirmed by XRD analysis. FTIR clear that changing the ratio of terbium and copper ions did not affect the locations of the borate and silicate groups, but it affected the intensity of absorption and amount of BO4, SiO4 and BO3 groups. The UV–visible–NIR spectra of the glasses showed a strong absorption of Tb^{3+} ions in the NIR region (2190, 1942, 1867, and 1775 nm for samples free of copper). The highest band gap value was obtained for the sample free of copper glass, which had the lowest amount of non-bridging oxygen. The estimated CIE coordinates for the glasses show their locations in the blue–green region for samples free from copper when excited at 250 nm and green when the sample was excited at 378 nm. And move to green region with the copper content increased. The CIE coordinates deviated towards the yellow region when excited at 378 nm and became green yellowish with increasing Tb concentration.

Keywords Terbium lithium zinc borate glass containing copper · UV–visible–NIR · Optical properties · CIE coordinates

✉ I. Kashif
ismailkashif52@yahoo.com; ismailkashif@azhar.edu.eg

[1] Department of Physics, Faculty of Science, Al-Azhar University, Nasr City, Cairo, Egypt

[2] Department of Physics, Faculty of Women for Arts, Science and Education, Ain Shams University, Heliopolis, Cairo, Egypt

Introduction

Glass prepared using a simple quenching method is easier to prepare than the crystal material, which saves time. Additionally, the ability of soluble rare earth (RE) and transition metal (TM) can be used in transparent media. Glass can drop different amounts of RE and different types that give the chance of high intensity emission in different colors. From literature studied a transparent glass doped with different RE as in Er_2O_3 gives green emission as studied by Prabhu [1], Kaurvv [2], Deopa [3]. Glass doped with Sm_2O_3 has a different range of red color as Swapna [4], Marzouk [5] and Eu_2O_3 in red emission as Hegde [6], Hegde [7], and Tm_2O_3 in blue emission El-Maaref [8] and Vijaya Babu, Cole [9] and Tb_4O_7 in green emission by Kaur [10] and Pr_6O_{11} Mahamuda [11], Hegde [12] and studied effect of different RE on mixed together Zhao [13], Sasikala [14], Mungra [15], Zhu [16], He [17], Hegde [18].

The preparation glass using a former has the advantage of low melting point, good solubility of RE and TM, outstanding thermal and chemical stabilities, and broad emission, making it most suitable for high-gain laser applications [19], and is inexpensive and relatively stable [20] like borate. In contrast, borate has a high phonon energy, which provides a good opportunity to overcome this problem through the addition of ZnO. The ability of ZnO as a heavy metal to reduce phonon energy has been reported [21] and decreases the hygroscopic properties with improvement in electrical, mechanical, thermal, and optical properties [10]. In addition, ZnO exhibits a high thermal resistance against crystallization [22]. The addition of silicate as a former in the formation of borosilicate glass offers various advantages, such as preventing crystallization and increasing the emission intensity [23]. Borosilicate glass was chosen because it combines the high stability of silicate with ability to lower the melting

Published online: 19 July 2024

temperature of borate [24]. Additionally, the use of borosilicate glass prevents heavy concentration quenching, which improves the efficiency of luminescence materials [25].

Choosing Rare earths such as Tb_4O_7 and transition metals such as CuO have, the ability to emit green light [26] in addition to their ability to be used in optoelectronic devices [27] and used in green lasers. Tb^{3+} doped glasses have been used in the development of electromagnetic transmission window of sea water, efficient green emitting phosphors, solid state lasers, white LED's, neutron detection, and medical devices [28] and a little in blue emission that give the chance to characterize the type of material like clustering of normal from the ratio between green intensity to blue intensity. Adding CuO can be used as two ways as the filter-pass or photoluminescence emission depend on the type of the host [29] that copper oxidation formed in prepared glass. This advantage give the chance of glass used as the glass filter when Cu^{2+} formed inside the network [30] or used in the emission when the Cu^{+} formed and wide luminescence in the visible region with a d9s → d10 transition in solids[19, 30–32].

Incorporating SiO_2 into the B_2O_3 glass matrix improves the heat resistance, chemical durability, and electrical resistivity of borosilicate glasses [33–36]. These glasses exhibit similar optical properties to fluoride glasses but offer better chemical resistance and superior mechanical properties. The narrow-band emission of Terbium (3+): Tb^{3+} arises from the transitions between the 4f levels. Trivalent terbium ions, Tb^{3+}, which results in sharp luminescence from 4f to 4f transitions. This sharpness is attributed to the shielding of the 4f electrons by the outer 5s2 and 5p6 orbitals. The green light emission in terbium ions [37–39] is attributed to four distinct peaks arising from the $^5D_4$ to ^7F_J transitions, where J is 3, 4, or 6. The most prominent green emission peak occurs at 544–550 nm within the visible light spectrum, suggesting its potential for use in electronic devices. Optical rays that emit light and lasers that emit green light [40, 41].

Our interest was focused on determining the effect of the substitution of Tb^{3+} ions and CuO emitted in green and some blue emission on the photoluminescence properties.

Experimental work

Glass samples with a composition of 35 SiO_2 + 35 B_2O_3 + 10 ZnO + 20 Li_2O + (1 − X) Tb_4O_7 + X CuO (where X = 0, 0.05, 0.1, 0.3, 0.5, and 1 mol% coded as Tb–Cu1, Tb–Cu_2, Tb–Cu_3, Tb–Cu_4, Tb–Cu_5, and Tb–Cu6, respectively. The glass samples under investigation were mounted with reagent grade SiO_2 (Sigma-Aldrich, 99.9%), H_3BO_3 (Win LAB U.K., 99%), ZnO (Sigma-Aldrich, 99.9%), CuO (Sigma-Aldrich, 99.9%), and Tb_4O_7 (Strem chemicals USA, 99.99).

The chemical purity grades were mixed and annealed for 30 min at 450 °C in a porcelain crucible and then melted at 1130 °C. The molten material was cooled and poured between two copper plates in air and annealed at 350 °C for 3 h. All the samples were examined using a Philips Analytical X-ray analysis system (PW3710) with Cu Kα = 1.54°A.

JASCO, V-570 spectrophotometer (with the precision of ± 1 nm), and JASCO FP-8300 spectrofluorometer (comprised of a 150 W Xenon arc lamp) measured the optical properties of glass samples (transmission, absorption, excitation, and emission).

Differential thermal analysis (DTA) of the prepared samples was performed in the temperature range of room temperature to 900 °C at a heating rate of 25 °C/min using Al_2O_3 powder as a reference material (Shimadzu DTA-50 analyzer).

Attenuated total reflection (ATR) FTIR spectra were obtained using ALPHA II FTIR spectrometer from Bruker Optik GmbH, Germany, equipped with diamond ATR crystal system in the spectral range of 4000–400 cm^{-1} with the resolution of 4 cm^{-1}.

Results and discussion

When examining the impact of one substance on another's properties, the following methods can be employed: substitution or addition. For oxide glass, a certain percentage of the oxide under study replaces an equivalent percentage of the original elements (substitution). In addition, a percentage of the oxide is added to the original glass composition without altering it, resulting in a total that exceeds 100% (addition). This methodology is documented in numerous scholarly papers [42–44].

Figure 1 illustrates the amorphous structure of the prepared glass, as determined by XRD measurements. The graph also reveals an increase in the peak amplitude at 25 °C, which is attributed to the increase in the copper concentration. This increase in copper concentration enable the glass to incorporate nanoparticles within its structure.

In our previous studies, we prepared samples of borosilicate glass in porcelain crucibles, at temperatures within the same limits. These samples were analyzed using an EDX device, which verifies the integrity of the samples. Porcelain crucibles react with lead oxide and some heavy elements, and it is recommended to avoid using them [45–47].

The infrared spectra of the glass samples are depicted in Fig. 2. The FTIR spectra disclose the structural configuration of the units within the glass samples. Additionally, the FTIR offers data on the stretching and bending vibrations for the silicon and boron groups.

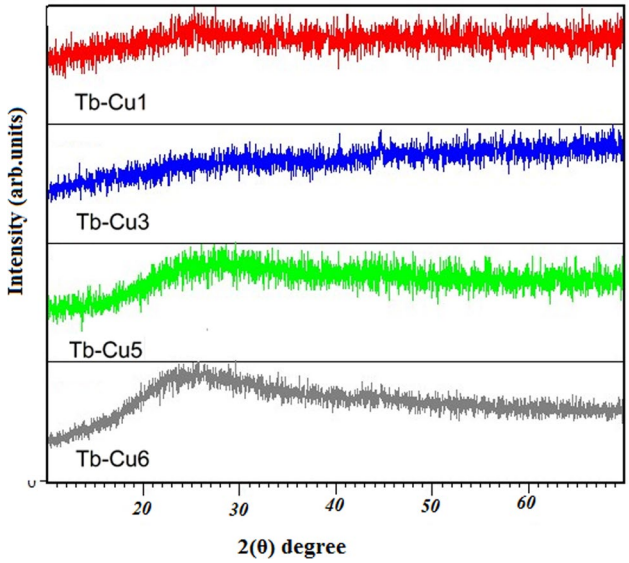

Fig. 1 The XRD of the prepared glass samples

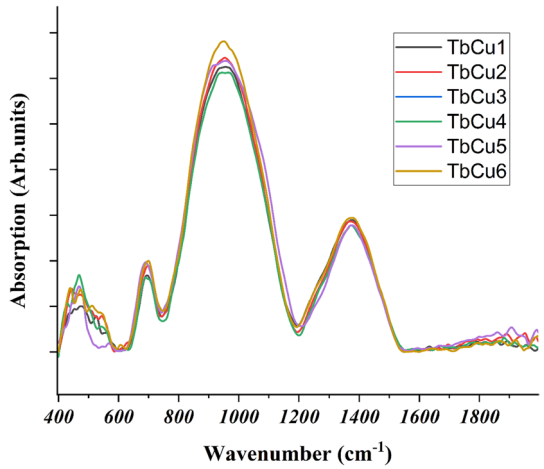

Fig. 2 The infrared spectra of the glass samples

All spectra demonstrate the presence of borate groups. The B–O stretching vibrations of trigonal $(BO_3)^{3-}$ units (in meta-, pyro-, and ortho-borate) cause the broad band from 1200 to 1700 cm^{-1}, centered at 1376 cm^{-1}. The anti-symmetrical stretching vibrations with three non-bridging oxygens (NBOs) of B–O–B linkages correspond to the band at 1420–1540 cm^{-1} [48]. The stretching vibrations of the non-bridging oxygen atoms (O–B–O) in the $[BO_2O]^-$ units, which are connected with $[BO_4]$ or $[BO_3]$ units, are found at 1360 cm^{-1} and 1455 cm^{-1}, respectively [49].

The spectral band between 800 and 1200 cm^{-1} is attributed to the stretching vibrations of B–O bonds in tetrahedral BO_4 units. The band around 1005 cm^{-1} is due to the non-bridging oxygens (NBOs) within the BO4 group. The silicate and borate groups —comprising BO_3 and BO_4 units—overlap their spectral contributions and may combine within the 1000–1120 cm^{-1} range.

The stretching vibration of Si–O–Si bonds in the NBO of SiO4 tetrahedral units causes two bands at 1040 and 1100 cm^{-1}. That is, as the NBO bonds (Si–O–Si links in Q1 units) rose, so did the bridge oxygen bond (Si–O–Si bonds) [48]. The stretching vibrations of Si–O–Si bonds in silicates result in various configurations in the glassy network. These configurations include Q3 (1075 cm^{-1}) with 3 bridging oxygen and one non-bridging, Q2 (1000 cm^{-1}) with 2 bridging oxygen and 2 non-bridging, and Q1 (900 cm^{-1}) with 1 bridging oxygen and 3 non-bridging. The band indicates the presence of B-O-Si bonds at 1020 cm^{-1}. The stretching vibration of Si–O–Si bonds in the non-bridging oxygen of SiO4 tetrahedral units produces two bands at 1040 and 1100 cm^{-1}. Fig. 3 shows the effect of Tb_4O_7 addition on the SiO4, BO4 and BO3 vibration groups. It is clear the structure variation between samples.

Figure 4a shows the effect of light fall on the sample in the UV, Vis, and near IR ranges. High-intensity peaks were observed in the NIR range for the sample doped with 1 mol% Tb_4O_7, followed by a decrease in the NIR range with the appearance of a peak at vis, which increased with

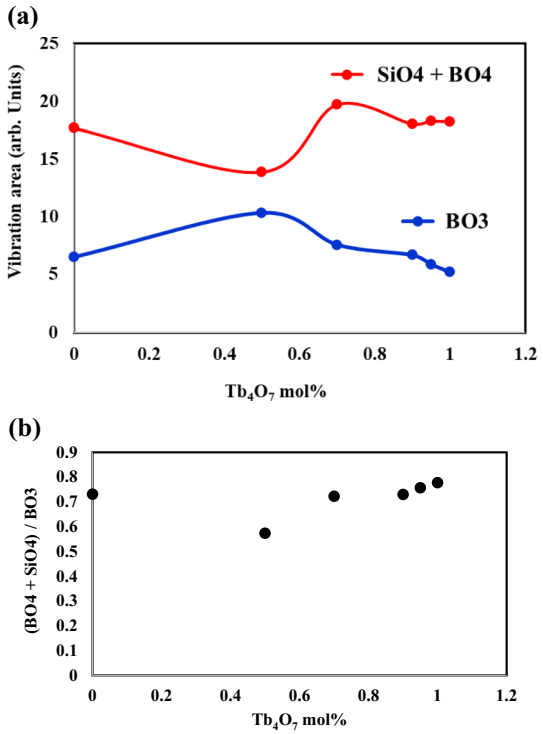

Fig. 3 **a** The BO_3 and $(BO_4+S_iO_4)$ **b** $(BO_4+S_iO_4)/BO_3$ value of prepared glass samples

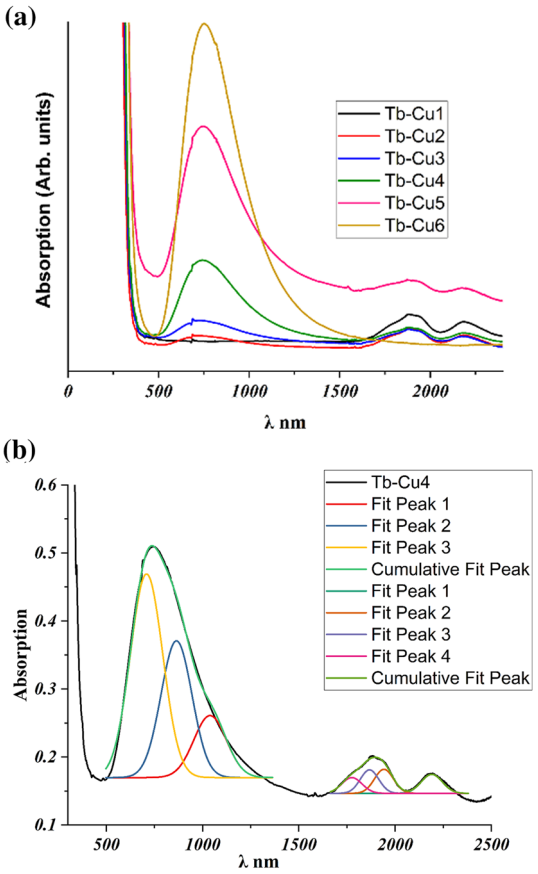

Fig. 4 **a** The UV–Vis–near IR of the glass samples. **b** The deconvolution of the glass sample 0.7 Tb_4O_7 and 0.3CuO

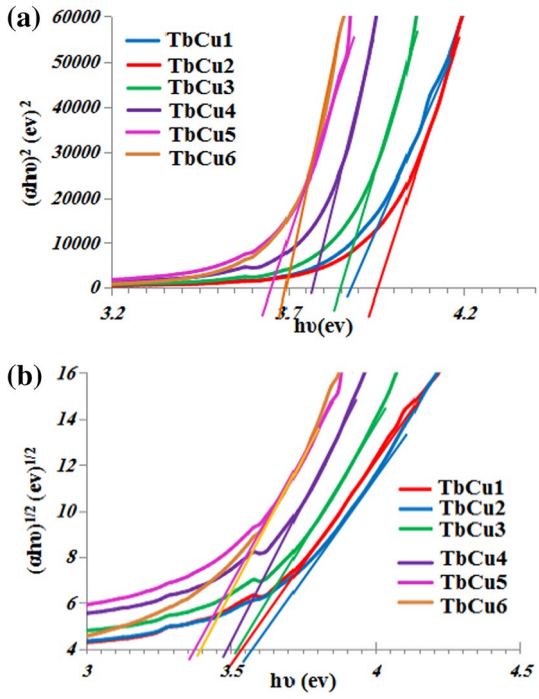

Fig. 5 The Tauc plot evaluated the **a** direct and **b** indirect Eg values

increasing Cu concentration. Using the deconvolution method shown in Fig. 4b, the positions of the peaks were determined. The appearance of peaks in the NIR range at 2190, 1942, 1867and 1775 nm are represented as $^7F_6 \rightarrow {}^7F_3$, $^7F_2$, $^7F_1$, and $^7F_0$ respectively [50–52]. The UV spectra contribute to the appearance of two low-intensity peaks at 486 and 379 nm, which represent transitions from $^7F_6$ to $^5D_4$ and $^5D_3$, respectively [51]. Generally, copper (Cu) exists in two valence states, Cu^+ and Cu^{2+}. The presence of Cu^+ is a result of the $\mathbf{3}d^{10} \rightarrow \mathbf{3}d^9$ 4S1 transition, which appears in the blue UV absorption spectrum and is observed in glass containing 0.5 and 1 mol % CuO.

During the melting process, the presence of Cu^{2+} results in octahedral coordination. This leads to splitting of the d orbitals into two degenerate T2g levels at a lower energy and a higher energy level of 2Eg. Additionally, tetragonal distortion causes the Jahn–Teller effect, resulting in the splitting of T2g ions into ^{2}B2g (dxy) and ^{2}Eg (dxz, dyz), whereas ^{2}Eg splits into ^{2}B2g (dx2–y2) and ^{2}A2g (dz2).

According to, [53] the appearance of a broad band is due to $^2\text{Eg} \rightarrow {}^2\text{B1g}$, $^2\text{B2g} \rightarrow {}^2\text{B1g}$, and $^2\text{A1g} \rightarrow {}^2\text{B1g}$, which correspond to 709, 864, and 1039 nm, respectively [54]. The intensity and broadness of the peak increased with increasing Cu concentration, and Cu^+ appears as previously observed, causing a decrease in the Tb peak intensity [32, 55].

To determine the physical transitions of light between the valence and conduction bands as Eg, we used optical absorption values. The value found by Mott and Davis is related to various parameters, including the absorption coefficient, photon energy, and optical band gap. The optical band gap is determined by the following relation [56].

$$\alpha h\upsilon = B(h\upsilon - Eg)^n \quad (1)$$

From the Tauc plot as shown in Fig. 5a and 5b, the direct and indirect Eg values were evaluated, where α represents the absorption coefficient, Eg is the optical band gap, and n is the optical transition of the electron. Generally, the addition of a modifier causes changes in the Eg values. This is because the modifier alters the NBOs present in the valence band, thereby forming extrinsic bands between them on the lattice and changing the distance between the valence and conduction bands.

The results obtained drawn in Fig. 6 indicate that glass containing rare earth (RE) has a high value of Eg, which decreases with an increase in transition metal content, consistent with literature sources [10, 55, 57, 58]. Furthermore,

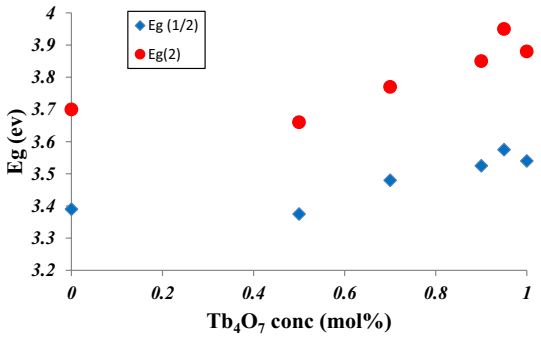

Fig. 6 The relation between Tb_4O_7 concentration and the Eg value at n = 1/2 and 2

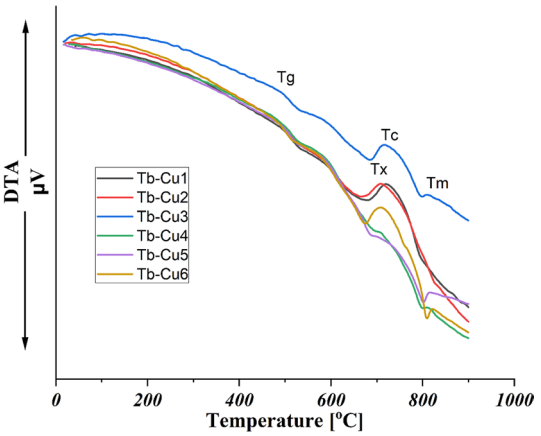

Fig. 7 The DTA curve of the prepared glass samples

as observed in studies [31, 59], adding Cu leads to a decrease in Eg.

This behavior can be attributed to structural changes. A decrease in BO4 units leads to an increase in NBO bonds, which in turn raises the electronic polarizability across the B–O bonds. Notably, an increase in NBOs narrows the band gap between the valence and conduction bands, resulting in a glass with low energy gap and high refractive index. This can also be linked to changes in bonding strength, which are influenced by ionic radius and electronegativity (Tb^{3+} = 0.106–0.118 and Cu^{3+}–Cu^{1+} = 0.068–0.091 nm). Furthermore, an increase in CuO relative to Tb_4O_7 leads to a reduction in BO4 formation and consequently, a decrease in Eg. The optical band gap behavior is generally nonlinear, a trend that can be attributed to the influence of mixed rare-earth and transition elements on the glass network. Additionally, reducing Tb and adding Cu can increase the donor centers, thereby lowering the Eg of the glasses. The smooth absorption edges in the absorption spectra indicate the amorphous nature of the current glass samples, a finding supported by density results [60]. Optical band gap values similar to those for borate glass systems containing dysprosium ions or transition metals [61, 62].

The DTA curve in Fig. 7 illustrates the thermal behavior of the prepared material with increasing temperature. The temperature increase exhibited an endothermic peak, indicating a glass transition temperature (Tg). As the temperature continued to increase, an exothermic peak appeared at the beginning of the crystallization nucleation peak (Tc) at the onset of the crystallization temperature Tx.

The temperature then increased continuously and another endothermic peak appeared, which corresponded to the melting glass temperature (Tm).

Table 1 lists the values of Tg, Tc, Tm, the Kauzmann relation Trg and the glass ability ΔT.

From the Tg values, a slight difference in value appears between the samples, and at the same time, a change in values is expected from the structural change in BOs and NBOs [53]. Glasses with higher BO3 content have a lower Tg [52]. To compare the samples prepared previously with different formers and increasing Cu concentrations [29, 63, 64]. These values agree with the results of the samples under study.

The glass transition temperature (Tg) decreases with the addition of copper, which modifies the glass structure owing to the increase in non-bridging oxygen sites (NBOS). The proximity of the crystallization temperature (Tc) to Tg or the melting temperature (Tm) explains the thermal stability and difficulty of crystallization. The ability of glass to delay crystallization and its good glass-forming ability are due to its stability in performance, with Tc closer to Tm than Tg. The difference between Tc or Tx and Tg, was calculated

Table 1 The DTA parameters (glass transition temperature Tg, crystallization temperature Tc and the melting temperature Tm), the Kauzmann relation Trg and the glass's ability ΔT

Tb_4O_7 (mol%)	Tg °C	Tx °C	Tc °C	Tm °C	Trg	ΔT °C
1	496	679.36	722.08	793	0.625	183
0.95	502	682.69	708.92	823.7	0.609	180
0.9	488	687.17	714	794.86	0.613	199
0.7	496.5	693.53	709.8	797	0.622	197
0.5	493.5	685	732	800	0.616	191
0	484.98	677.64	707.54	807.85	0.600	192

to determine ΔT [64]. Another important factor is the estimation of the glass-forming ability using the Kauzmann relation Trg = Tg/Tm, which was calculated using the DTA parameter.

By obtaining a value of Trg within the range of 0.5 to 0.66, the system identifies the glass with the highest value that has good forming ability.

In Figs. 8 and 9, the excitation spectra obtained by varying the wavelength of the Cu ions to 460 nm and that of the Tb^{3+} ions to 543 nm. When glass samples are excited with Tb ions at 543 nm, different excitation peaks can be observed in the ultraviolet (UV), near-ultraviolet (n-UV), and blue regions. The spectra displayed six excitation bands, with peaks at 304, 318, 342, 352, 370, 378, and 486 nm attributed to the transitions from the ground level ($^7F_6$) to $^5H_4$, $^5H_7 + {}^5D_1$, $^5L_{6,7}$, $^5G_5$, $^5L_{10}$, $^5G_6 + {}^5D_3$, and $^5D_4$ excited states, respectively [65, 66] at different positions.

Figure 8 shows a reduction in the peak intensity as the concentration of Tb_4O_7 decreased. Moreover, all peaks disappeared in the glass samples containing only CuO. If we choose to excite Cu ions at 460 nm and record the excitation spectrum in the UV range, as shown in Fig. 9, the peak at 250 nm represents the transition from ^{1}Ag to ^{1}T2g of Cu^+. As the intensity of the peak changed, the decrease indicated an improvement in Cu^{2+} [32].

The light produced by Tb^{3+} ions can be divided into two regions based on the excited level emitted. When the excited level emitted was $^5D_3$ to $^7F_{6\text{-}3}$, emission peaks observed at wavelengths less than 480 nm were observed at 382, 416, 438, and 480 nm, characterized by blue emission. In contrast, the closest level to $^5D_3$ is $^5D_4$, which allows non-radiative energy to increase the emission at 488, 545, 588, and 622. These emissions are formed as a transition to a lower level ($^5D_4$ to $^7F_{6\text{-}3}$) as green emissions [67, 68]. According to previous studies, the sum of the emission intensity results from the excited level $^5D_4$ to the emission intensity resulting from the excited state $^5D_3$ indicates the distribution of Tb in a glass sample.

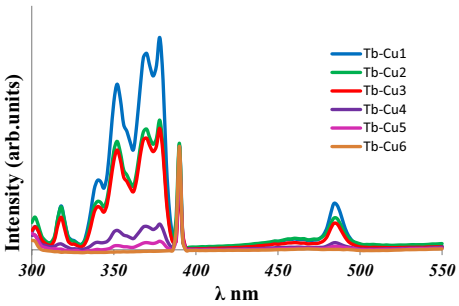

Fig. 8 The excitation curve of glass samples at $\lambda_{em} = 543$ nm

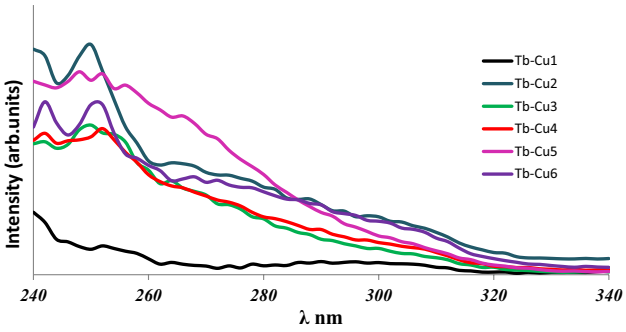

Fig. 9 The excitation curve of glass samples at $\lambda_{em} = 460$ nm

This distribution can be either homogeneous or clustered [28, 67, 69–71].The disappearance of the blue emission is a sign of clustering of Tb ions in the glass sample. However, the increase in green emission suggests that glass may be suitable for green laser applications [10]. According to our research, the emission of Cu ions is explained by the presence of Cu^+ in both its + 3 and + 2 charge states, which act as luminescence centers (also known as defect centers) that enhance phosphor emission intensity [29]. When present as Cu^+ (3d9-4S1), Cu ions act as color centers, which are utilized in the emission properties. In contrast, the presence of Cu^{2+} has an inverse effect on emissions [20].

From the excitation curve (Fig. 8), it can be observed that the highest intensity occurred at 378 nm. This indicates the most suitable wavelength for exciting Tb^{3+}ions. Figure 10 shows the emission of the glass sample under 378 nm excitation. It shows high-intensity peaks in the green emission region, and low-intensity peaks in the blue emission region.

The glass sample doped with CuO did not show any Cu emission and its peaks disappeared. The figure shows that the emission intensity decreased with decreasing Tb_4O_7 concentration. Because there was no emission of Cu ions, we

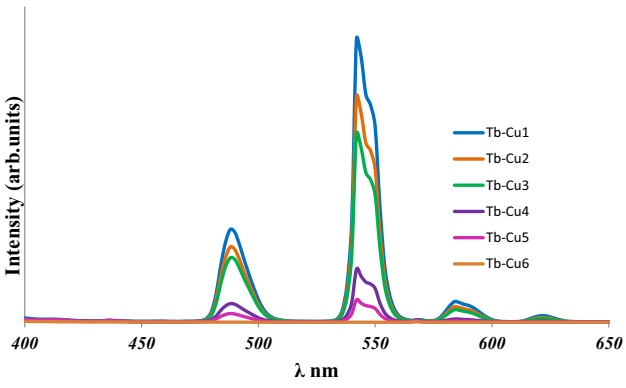

Fig. 10 The emission spectra of glass samples doped with different concentration of CuO and Tb_4O_7 excited at $\lambda_{ex} = 378$ nm

Table 2 The peaks intensity of transition ($^5D_3$-^7F_J) and ($^5D_4$-^7F_J)

sample	Intensity ($^5D_3$-^7F_J)		ΣI($^5D_3$)	Intensity ($^5D_4$-^7F_J)				ΣI($^5D_4$)	ΣI($^5D_4$)/ΣI($^5D_3$)
	$^7F_5$	$^7F_4$		$^7F_6$	$^7F_5$	$^7F_4$	$^7F_3$		
Tb-Cu1	5.4	3.27	8.67	176	537.84	38.86	10.8	763.5	88.06
Tb-Cu2	3.4	2.4	5.8	142.85	428.29	29.22	8.37	608.73	104.95
Tb-Cu3	3.7	3.04	6.74	121.99	357.93	22.35	6.29	508.56	75.45
Tb-Cu4	3.7	2.4	6.1	34.93	100.36	5.5	1.27	142.06	23.28
Tb-Cu5	4.17	2.8	6.97	16.11	42.1	1.9	0.32	60.43	8.67

Table 3 Density, molar volume, number of Tb3+ ions in unit volume and distance between Tb^{3+} ions

Sample	Density (g/cm^3)	Molar volume (cm^3/mol)	N E + 24 (No./cm^3)	R (nm)
Tb-Cu1	2.735	24.489	6.727	0.53
Tb-Cu2	2.724	24.465	6.371	0.539
Tb-Cu3	2.741	24.194	6.141	0.546
Tb-Cu4	2.701	24.063	4.731	0.596
Tb-Cu5	2.646	24.052	3.313	0.671
Tb-Cu6	2.539	23.756	–	–

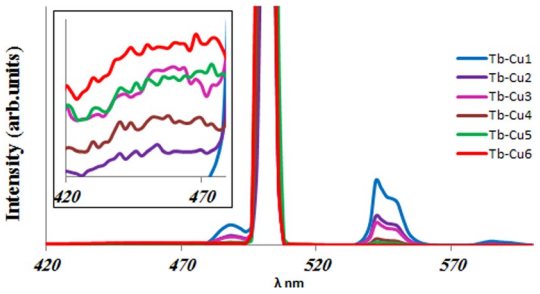

Fig. 11 The emission spectra of glass samples doped with different concentration of CuO and Tb_4O_7 excited at λexc = 250 nm

determined the distribution of Tb^{3+} ions inside the network. The intensity ratio of green to blue is a sensitive parameter that can be used to determine the concentration of Tb_4O_7.

Table 2 shows the calculated ratio between the sum of the intensities of the green emission ($^5D_4$-^7F_J) and the sum of the peak intensity of the blue emission ($^5D_3$-^7F_J). The obtained values indicate an increase in the value for the sample containing 0.95 mol% Tb_4O_7, suggesting that the Tb^{3+} ions are clustered. As the concentration of Tb_4O_7 decreased, the ratio began to decrease, explaining the increase in blue emission and indicating a more homogeneous distribution of Tb^{3+} ions at low concentrations of Tb_4O_7 [68].

From the perspective of bridging oxygen BO and NBOs, density plays an important role in characterizing the glass structure.

The effect of Tb_4O_7 concentration on density and molar volume is seen in Table 3.

The density ρ and molar volume Vm {Molar volume = molecular weight/ density (Vm = Mw/ρ)} exhibit a similar tendency in this picture, with the density and Vm increasing as the Tb_4O_7 concentration increases. Tb^{3+} enters the interstitial position in the glass structure, breaks bonds to create NBOs, and causes a volume increase. The density increased as the M_W (molecular weight) of Tb increased. Vm increases as the oxygen level rises, resulting in the depolymerization of glass structures. From density and molar volume calculate the number of Tb^{3+} ions per unit volume according to N = (DρNA)/Mw {D is the concentration of Tb_4O_7, NA is the Avogadro's number}, also the distance between Tb^{3+}–Tb^{3+} ions calculated using the relation $R=\left(\frac{1}{N}\right)^{1/3}$. And set in Table 3. From it, can be observed that the Tb^{3+} ions are too far from each other, disallowing excitation energy to be transmitted between surrounding rare-earth ions, resulting in an increase in emission intensity and increase in radiative energy.

Figure 10 shows a high-intensity peak at 542 nm, which exhibits splitting. This phenomenon is caused by the distortion of the glass network by Tb^{3+} ions, which leads to a stark splitting of the energy level [28].

Based on the excitation curve of Cu shown in Fig. 9, the excitation wavelength of the Cu ions was chosen as 250 nm to excite the glass samples, as shown in Fig. 11.

Figure 11 shows the ability to excite Tb^{3+} ions and its effect on the peaks of 488, 542, and 584 nm of green emission. The high-intensity peak of Tb_4O_7 emission decreases and appears as the emission of a broad emission peak of Cu ions with the increase in Cu concentration. This decrease in the intensity of the peak in the green region reduced the ratio between the green and blue regions. In addition, the very towering peaks inside the broadband at 502 nm represent the boron emission. The towering peak

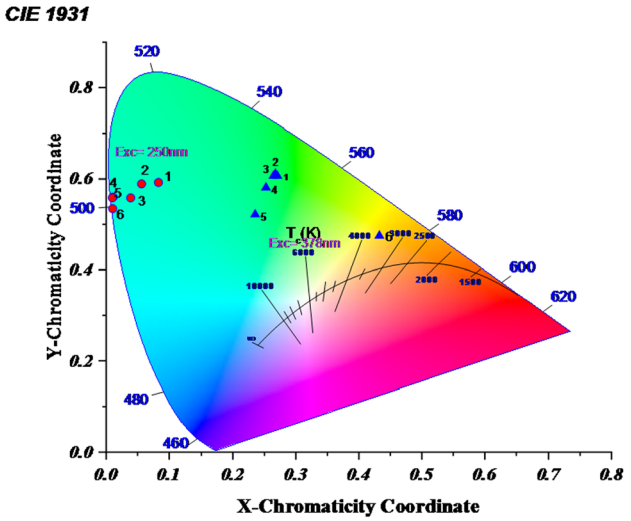

Fig. 12 CIE1931 chromaticity coordinates for glasses under excitation wavelength at 250 nm and 378 nm

represents the contribution of boron emission, which was previously studied by Lu [72, 73], Collins [74] and Freitas [75]. The broad band signifies the emission mechanism formed by Cu, as when the glasses are excited at 250 nm, the excited electrons populate the higher 1T2g level, and non-radiative relaxation to the 3Eg level occurs. The short life span of this level, from radiative relaxation to the 1Ag ground level appears a broad emission peak of around 470 nm [32, 76].

The color of the glass sample varied from that under day light or UV excitation light. The visible emission color under UV light was evaluated using the CIE chromaticity coordinates. The emitted color when different emission wavelengths are mixed as shown in Figs. 10 and 11 is shown in Fig. 12.

From Fig. 12, shows differences in the emitted colors under different UV lights. The sample excited at 378 nm shows green emission, which is in accordance with a previous report [28, 53, 66], whereas under 250 nm, the green emission is italicized to blue-green. The obtained data for the corresponding (x, y) coordinates are listed in Table 4. The second vital parameter determination is CCT [32, 66] by

$$CCT = -449\upsilon 3 + 3525\upsilon 2 - 6823.2\upsilon + 5520.3$$

where $\upsilon = (x\text{-}0.332)/(y\text{-}0.186)$. The evaluated values are tabulated in Table 4.

This shows the difference in color brightness with different Tb_4O_7 concentrations and the ability to use samples doped with Tb_4O_7 and CuO in daylight fluorescence and samples doped with Cu in neutral-white fluorescence.

Conclusion

Terbium lithium zinc borosilicate glass doped with copper oxide was prepared using a melting technique. The spectroscopic characteristics of the obtained glass systems were examined by recording their excitation and emission spectra. When directly excited, the characteristic luminescence bands arising from the electronic transitions of the Tb^{3+} ions were observed. Further experiments were conducted to investigate the impact of copper ion concentration on the spectroscopic characteristics of lithium zinc borate glasses. They found that under UV–visible light excitation, our glass system displays different colors between blue, green, and yellow emissions, which is the result of multiple bands of Tb^{3+} forming simultaneously. The results indicate that lithium zinc borate glasses can be used as potential light emitters.

Table 4 The chromaticity parameter (x,y) and the correlated temperature CCT

Sample	Exc at 378 nm			Exc at 250 nm		
	x	Y	CCT	x	Y	CCT
TbCu1	0.270	0.606	6592	0.083	0.592	11,128
TbCu2	0.267	0.611	6637	0.056	0.589	11,982
TbCu3	0.264	0.606	6709	0.038	0.558	13,286
TbCu4	0.252	0.581	7038	0.010	0.560	14,256
TbCu5	0.235	0.521	7787	0.009	0.558	14,342
TbCu6	0.432	0.474	3552	0.010	0.534	15,172

Acknowledgements The authors thank Material Science and Glass research Lab., Physics Department, Faculty of science, AL-AZHAR University for providing the measurement facilities.

Author contributions AR: investigation, writing—original draft, methodology, formal analysis. IK: writing—review and editing, administration, formal analysis, investigation. SSA: preparation samples, measurements, writing draft. NMK: preparation samples, measurements, writing draft. MAE: preparation samples, measurements, writing draft.

Funding No funding for research.

Data availability No data was used for the research described in the article.

Declarations

Ethical approval This paper meets the ethical standards of this journal.

Consent to participate All authors agree with the review of this paper in this journal.

Competing interests The authors declare that they have no known competing financial interests or personal relationships that could have appeared to influence the work reported in this paper.

References:

1. N.S. Prabhu, A.N. Meza-Rocha, O. Soriano-Romero, U. Caldino, E.F. Huerta, C. Falcony, M.I. Sayyed, H. Al-Ghamdi, A.H. Almuqrin, S.D. Kamath, Spectroscopic study of Er3+ doped borate glass system for green emission device, NIR laser, and optical amplifier applications. J. Lumin. **238**, 118216 (2021). https://doi.org/10.1016/j.jlumin.2021.118216
2. S. Kaur, O.P. Pandey, C.K. Jayasankar, N. Chopra, Effect of gamma irradiation on physical, optical, spectroscopic and structural properties of Er3+-doped vitreous zinc borotellurite. J. Lumin. **235**, 118031 (2021). https://doi.org/10.1016/j.jlumin.2021.118031
3. N. Deopa, M.K. Sahu, S. Kaur, A. Prasad, K. Swapna, V. Kumar, R. Punia, A.S. Rao, Enhanced visible green and 1.5 μm radiative emission of Er3+ ions in Li2O-PbO-Al2O3-B2O3 glasses for photonic applications. J. Rare Earths **39**(5), 520–525 (2021). https://doi.org/10.1016/j.jre.2020.05.002
4. K. Swapna, Sk. Mahamuda, A.S. Rao, S. Shakya, T. Sasikala, D. Haranath, G.V. Prakash, Optical studies of Sm3+ ions doped Zinc Alumino Bismuth Borate glasses. Spectrochim. Acta Part A Mol. Biomol. Spectrosc. **125**, 53–60 (2014). https://doi.org/10.1016/j.saa.2014.01.025
5. M.A. Marzouk, H.A. Elbatal, A.M. Abdelghany, Effect of Gd_2O_3 and Sm_2O_3 addition on the properties of CeO_2. J. Korean Inst. Electr. Electron. Mater. Eng. **16**(11), 979–986 (2003). https://doi.org/10.4313/jkem.2003.16.11.979
6. V. Hegde, N. Chauhan, V. Kumar, C.S.D. Viswanath, K.K. Mahato, S.D. Kamath, Effects of high dose gamma irradiation on the optical properties of Eu3+ doped zinc sodium bismuth borate glasses for red LEDs. J. Lumin. **207**(2019), 288–300 (2019). https://doi.org/10.1016/j.jlumin.2018.11.023
7. V. Hegde, S.D. Kamath, I. Kebaili, M.I. Sayyed, K.N. Sathish, C.S.D. Viswanath, A.G. Pramod, P. Ramesh, K. Keshavamurthy, G. Devarajulu, G. Jagannath, Photoluminescence, nonlinear optical and gamma radiation shielding properties of high concentration of Eu2O3 doped heavy metal borate glasses. Optik (Stuttg) **251**, 168433 (2022). https://doi.org/10.1016/j.ijleo.2021.168433
8. A.A. El-Maaref, E.A. Abdel Wahab, Kh.S. Shaaban, M. Abdelawwad, M.S.I. Koubisy, J. Börcsök, E.S. Yousef, Visible and mid-infrared spectral emissions and radiative rates calculations of Tm3+ doped BBLC glass. Spectrochim. Acta Part A Mol. Biomol. Spectrosc. **242**, 118774 (2020). https://doi.org/10.1016/j.saa.2020.118774
9. K. Vijaya Babu, S. Cole, Luminescence properties of Dy3+-doped alkali lead alumino borosilicate glasses. Ceram. Int. **44**(8), 9080–9090 (2018). https://doi.org/10.1016/j.ceramint.2018.02.115
10. S. Kaur, N. Deopa, A. Prasad, R. Bajaj, A.S. Rao, Intense green emission from Tb^{3+} ions doped zinc lead alumino borate glasses for laser and w-LEDs applications. Opt. Mater. (Amst.) **4**, 318–323 (2018). https://doi.org/10.1016/j.optmat.2018.07.020
11. S. Mahamuda, K. Swapna, A. Srinivasa Rao, T. Sasikala, L. Rama Moorthy, Reddish-orange emission from Pr3+ doped zinc alumino bismuth borate glasses. Phys. B Condens. Matter **428**, 36–42 (2013). https://doi.org/10.1016/j.physb.2013.07.010
12. V. Hegde, C.S.D. Viswanath, N. Chauhan, K.K. Mahato, S.D. Kamath, Photoluminescence and thermally stimulated luminescence properties of Pr^{3+}-doped zinc sodium bismuth borate glasses. Opt. Mater. (Amst.) **84**, 268–277 (2018). https://doi.org/10.1016/j.optmat.2018.06.064
13. S. Zhao, F. Xin, Sh. Xu, D. Deng, L. Huang, H. Wang, Y. Hua, Luminescence properties and energy transfer of Eu/Tb ions codoped aluminoborosilicate glasses. J. Non Cryst. Solids **357**(11–13), 2424–2427 (2011). https://doi.org/10.1016/j.jnoncrysol.2010.11.092
14. T. Sasikala, L. Rama Moorthy, Photoluminescence properties of singly doped Tm^{3+} and co-doped Tm3+/Tb3+ions in tellurite glasses. J. Mol. Struct. **1076**, 529–534 (2014). https://doi.org/10.1016/j.molstruc.2014.07.051
15. M. Mungra, F. Steudel, B. Ahrens, S. Schweizer, Tm/Tb/Eu triple-doped lithium aluminoborate glass for white light generation. J. Lumin. **192**, 71–76 (2017). https://doi.org/10.1016/j.jlumin.2017.06.028
16. C. Zhu, D. Wu, J. Liu, M. Zhang, Y. Zhang, Color-tunable luminescence in Ce-, Dy-, and Eu-doped oxyfluoride aluminoborosilicate glasses. J. Lumin. **183**, 32–38 (2017). https://doi.org/10.1016/j.jlumin.2016.11.004
17. D. He, Y. Fang, M. Liao, G. Zhao, Y. Sun, F. Yu, L. Hu, X. Wang, J. Hou, T. Xue, Y. Liu, Luminescence properties and energy transfer behavior of Dy3+/Tm 3+ co-doped phosphate glasses with high moisture-resistance and thermal stability for W-LEDs. J. Lumin. **236**, 118087 (2021). https://doi.org/10.1016/j.jlumin.2021.118087
18. V. Hegde, C.S.D. Viswanath, K.K. Mahato, S.D. Kamath, Warm white light and colour tunable characteristics of Dy^{3+} co-doped with Eu^{3+} and Pr^{3+} zinc sodium bismuth borate glasses for solid state lighting applications. Mater. Chem. Phys. **234**, 369–377 (2019). https://doi.org/10.1016/j.matchemphys.2019.05.063
19. P.R. Rani, M. Venkateswarlu, Sk. Mahamuda, K. Swapna, N. Deopa, A.S. Rao, G.V. Prakash, Structural, absorption and photoluminescence studies of Sm3+ ions doped barium lead alumino fluoro borate glasses for optoelectronic device applications. Mater. Res. Bull. **110**, 159–168 (2019). https://doi.org/10.1016/j.materresbull.2018.10.033
20. Y.S.M. Alajerami, S. Hashim, W.M.S. Wan Hassan, A.T. Ramli, M.A. Saleh, The effect of MgO on the optical properties of lithium sodium borate doped with Cu+ ions. Opt. Spectrosc. (Engl. Transl. Opt. i Spektrosk.) **114**(4), 537–543 (2013). https://doi.org/10.1134/S0030400X1304022X

21. M. Kumar, A.S. Rao, Influence of Tb3+ ions concentration and temperature on lithium bismuth alumino borosilicate glasses for green photonic device applications. Opt. Mater. (Amst.) **120**, 111439 (2021). https://doi.org/10.1016/j.optmat.2021.111439
22. A. Thulasiramudu, S. Buddhudu, Optical characterization of Cu2+ ion-doped zinc lead borate glasses. J. Quant. Spectrosc. Radiat. Transf. **97**(2), 181–194 (2006). https://doi.org/10.1016/j.jqsrt.2005.04.006
23. D. Aboutaleb, B. Safi, Structure and properties of the soda-borate glasses: effect of adding Fe2O3 concentration. J. Chem. Eng. Process Technol. **7**(1), 2–5 (2015). https://doi.org/10.4172/2157-7048.1000268
24. S. El-jadal, The influence of iron oxide on the structural and optical properties of borosilicate. Sci. J. Appl. Sci. Sabratha Univ. **9**, 33–46 (2022)
25. H. Wen, P.A. Tanner, Optical properties of 3d transition metal ion-doped sodium borosilicate glass. J. Alloys Compd. **625**, 328–335 (2015)
26. K. Tonooka, O. Nishimura, Effect of calcination temperature on the luminescent properties of Tb-doped borosilicate glasses. J. Mater. Sci. **34**(20), 5039–5044 (1999). https://doi.org/10.1023/A:1004792529119
27. I.R. Mohammed, A study on optical, spectroscopic and structural properties of copper-doped calcium lithium borate glasses. J. Opt. **49**(4), 556–563 (2020). https://doi.org/10.1007/s12596-020-00641-3
28. K. Swapna, S. Mahamuda, A.S. Rao, M. Jayasimhadri, S. Shakya, G.V. Prakash, Tb3+ doped Zinc Alumino Bismuth Borate glasses for green emitting luminescent devices. J. Lumin. **156**, 180–187 (2014). https://doi.org/10.1016/j.jlumin.2014.08.019
29. H.K. Obayes, H. Wagiran, R. Hussin, M.A. Saeed, Structural and optical properties of strontium/copper co-doped lithium borate glass system. Mater. Des. **94**, 121–131 (2016). https://doi.org/10.1016/j.matdes.2016.01.018
30. A. Okasha, S.Y. Marzouk, A.M. Abdelghany, Design a tunable glasses optical filters using CuO doped fluoroborate glasses. Opt. Laser Technol. **137**, 106829 (2021). https://doi.org/10.1016/j.optlastec.2020.106829
31. Y. Shi, R. Wei, J. Guo, X. Tian, F. Hu, H. Guo, Influence of optical basicity on Cu+ luminescence in aluminosilicate oxyfluoride glasses. Front. Mater. **6**, 1–6 (2019). https://doi.org/10.3389/fmats.2019.00246
32. O. Soriano-Romero, R. Lozada-Morales, A.N. Meza-Rocha, S. Carmona-Tellez, U. Caldino, B. Flores-Desirena, R. Palomino-Merino, Cold bluish white and blue emissions in Cu+-doped zinc phosphate glasses. J. Lumin. **217**, 1–7 (2020). https://doi.org/10.1016/j.jlumin.2019.116791
33. W. Rittisut, P. Manyum, N. Wantana, Y. Ruangtaweep, S. Rujirawat, K. Kamonsuangkasem, R. Yimnirun, A. Prasatkhetragarn, S. Kothan, H.J. Kim, J. Kaewkhao, Synthesis and characterization of eco-friendly, stable green-emitting Tb^{3+}-doped borosilicate glasses using waste silica gel. J. Non Cryst. Solids **638**, 123045 (2024)
34. N. Singkiburin, N. Srisittipokakun, R. Rajaramakrishna, S. Kothan, N. Intachai, J. Kaewkhao, Investigation of europium oxide (Eu_2O_3) doped in cobalt boro-silicate glasses from waste glass for photonics material application. Optik (Stuttg) **291**, 171146 (2023)
35. M. Zhao, Q. Zhang, Z. Xia, Structural engineering of Eu2+-doped silicates phosphors for LED applications. Acc. Mater. Res. **1**(2), 137–145 (2020)
36. N. Intachai, S. Kothan, N. Wantana, S. Kaewjaeng, P. Pakawanit, N. Vittayakorn, P. Kanjanaboos, N. Phuphathanaphong, H.J. Kim, J. Kaewkhao, Eu_2O_3 doped silicoborate glasses for scintillation material application: luminescence ability and X-ray imaging. Optik (Stuttg) **294**, 171439 (2023)
37. Y.-C. Li, Y.-H. Chang, Y.-S. Chang, Y.-J. Lin, C.-H. Laing, Luminescence and energy transfer properties of Gd^{3+} and Tb^{3+} in LaAlGe2O7. J. Phys. Chem. C **111**(28), 10682–10688 (2007)
38. C.R. Kesavulu, H.J. Kim, S.W. Lee, J. Kaewkhao, E. Kaewnuam, N. Wantana, Luminescence properties and energy transfer from Gd^{3+} to Tb^{3+} ions in gadolinium calcium silicoborate glasses for green laser application. J. Alloys Compd. **704**, 557–564 (2017)
39. D. Valiev, E. Polisadov, S. Stepanov, K. Belikov, N. Yegorov, H. Othman, V. Vaganov, Luminescence spectroscopy of scintillating glasses doped with Tb^{3+}/Ce^{3+} with different concentrations of cerium under photo-and electron excitation. J. Lumin. **162**, 128–133 (2015)
40. C. Zu, Y. Wang, J. Chen, B. Han, H. Tao, Luminescent properties and applications of Tb^{3+} doped silicate glasses with industrial scales. J. Non Cryst. Solids **357**(11–13), 2435–2439 (2011)
41. Z. Chenggang, Z. Zhihua, Z. Ligang, X. Anguo, C. Yuandao, Z. Xiangyang, Z. Yongbing, L. Xiaoyang, G. Qizhi, Luminescence properties of Tb3+-doped borosilicate scintillating glass under UV excitation. Spectrochim. Acta Part A Mol. Biomol. Spectrosc. **147**, 324–327 (2015). https://doi.org/10.1016/j.saa.2015.03.097
42. I. Kashif, A. Ratep, Impact of europium ions Eu3+ on thermal, optical, and luminescence properties of lithium zinc borate glasses. Optik (Stuttg) **300**, 171621 (2024)
43. I. Kashif, A. Ratep, Various color light emission from single, double, and triple Eu 3+/Tb 3+/Tm 3+ doped borate glass excited by UV light. J. Fluoresc. (2023). https://doi.org/10.1007/s10895-023-03502-x
44. S. Dayioglugil, N. Solak, Effect of ZnO on luminescence performance of terbium-activated zinc borosilicate glasses. Materials (Basel) **17**(9), 2154 (2024)
45. I. Kashif, M.L. Montes, M.A. Taylor, A. Ratep, Influence of Fe substitution on the Eu-doped lithium borosilicate glass system's physical, thermal, magnetic, and luminescent properties. J. Mater. Sci. Mater. Electron. **35**(4), 1–15 (2024)
46. I. Kashif, A. Ratep, Effect of addition of dysprosium oxide on spectroscopic properties and Judd-Ofelt analysis of lithium borosilicate glass system. SILICON **15**(7), 3365–3378 (2023). https://doi.org/10.1007/s12633-022-02249-7
47. I. Kashif, A. Ratep, Judd–Ofelt and luminescence study of Dysprosium-doped lithium borosilicate glasses for lasers and w-LEDs. Boletín la Soc. Española Cerámica y Vidr. **61**(6), 622–633 (2022)
48. R. Kaur, S. Singh, O.P. Pandey, Influence of CdO and gamma irradiation on the infrared absorption spectra of borosilicate glass. J. Mol. Struct. **1049**, 409–413 (2013). https://doi.org/10.1016/j.molstruc.2013.06.072
49. Y. Lai, Y. Zeng, X. Tang, H. Zhang, J. Han, H. Su, Structural investigation of calcium borosilicate glasses with varying Si/Ca ratios by infrared and Raman spectroscopy. RSC Adv. **6**(96), 93722–93728 (2016). https://doi.org/10.1039/c6ra20969f
50. T. Sambasiva Rao, D.V.K. Reddy, S.K. Taherunnisa, A.S.S. Reddy, P.V. Rao, N. Veeraiah, M.R. Reddy, Studies on structural characterization and near white light emission through energy transfer between Ce3+ and Tb3+ in barium gallium borosilicate glasses. J. Mol. Struct. **1190**, 184–195 (2019). https://doi.org/10.1016/j.molstruc.2019.04.065
51. V.X. Quang, P. Van Do, N.X. Ca, L.D. Thanh, V.P. Tuyen, P.M. Tan, V.X. Hoa, N.T. Hien, Role of modifier ion radius in luminescence enhancement from 5D4 level of Tb3+ ion doped alkali-alumino-telluroborate glasses. J. Lumin. **221**, 117039 (2020). https://doi.org/10.1016/j.jlumin.2020.117039
52. S.N.S. Yaacob, M.R. Sahar, E.S. Sazali, Z.A. Mahraz, K. Sulhadi, Comprehensive study on compositional modification of Tb3+ doped zinc phosphate glass. Solid State Sci. **81**, 51–57 (2018). https://doi.org/10.1016/j.solidstatesciences.2018.05.006

53. E.O. Taha, A. Saeed, The effect of cobalt/copper ions on the structural, thermal, optical, and emission properties of erbium zinc lead borate glasses. Sci. Rep. **13**(1), 1–13 (2023). https://doi.org/10.1038/s41598-023-39256-6
54. I. Kashif, A. Ratep, Blue, red, and green emission from chromium and copper metal doped lithium borate glass. IOP Conf. Ser. Mater. Sci. Eng. (2020). https://doi.org/10.1088/1757-899X/956/1/012013
55. G. Sangeetha, K.C. Sekhar, A. Hameed, G. Ramadevudu, M.N. Chary, M. Shareefuddin, Influence of CaO on the structure of zinc sodium tetra borate glasses containing Cu2+ ions. J. Non Cryst. Solids **563**, 120784 (2021). https://doi.org/10.1016/j.jnoncrysol.2021.120784
56. I. Kashif, H. Farouk, A. Ratep, M. Al Mahalawy, White light emission in Dy^{3+} doped SiO2B2O3Bi2O3TeO2 glass system. J. Non Cryst. Solids **522**, 119581 (2019). https://doi.org/10.1016/j.jnoncrysol.2019.119581
57. Y.S. Mustafa Alajerami, S. Hashim, W.M. Saridan Wan Hassan, A.T. Ramli, The effect of CuO and MgO impurities on the optical properties of lithium potassium borate glass. Phys. B Condens. Matter **407**(13), 2390–2397 (2012). https://doi.org/10.1016/j.physb.2012.03.029
58. O.A. Zamyatin, V.G. Plotnichenko, M.F. Churbanov, E.V. Zamyatina, V.V. Karzanov, Optical properties of zinc tellurite glasses doped with Cu_2 + ions. J. Non Cryst. Solids **480**, 81–89 (2018). https://doi.org/10.1016/j.jnoncrysol.2017.08.025
59. H. Aboud, H. Wagiran, I. Hossain, R. Hussin, S. Saber, M. Aziz, Effect of co-doped S_nO_2 nanoparticles on the optical properties of Cu-doped lithium potassium borate glass. Mater. Lett. **85**, 21–24 (2012). https://doi.org/10.1016/j.matlet.2012.06.033
60. P.P. Pawar, S.R. Munishwar, D.D. Ramteke, R.S. Gedam, Physical, structural, thermal and spectroscopic investigation of Sm_2O_3 doped LAB glasses for orange LED. J. Lumin. **208**, 443–452 (2019)
61. A. Ichoja, S. Hashim, S.K. Ghoshal, I.H. Hashim, R.S. Omar, Physical, structural and optical studies on magnesium borate glasses doped with dysprosium ion. J. Rare Earths **36**(12), 1264–1271 (2018)
62. M. Abdel-Baki, F.A. Abdel-Wahab, F. El-Diasty, One-photon band gap engineering of borate glass doped with ZnO for photonics applications. J. Appl. Phys. **111**(7), 073506 (2012)
63. Y. Shang, M. Wang, E. Li, C. Zhong, T. Qin, Enhancing thermal and dielectric properties of $MgO–Al_2O_3–S_iO_2–B_2O_3$ glass-ceramics through CuO doping. Ceram. Int. **49**(19), 32078–32085 (2023). https://doi.org/10.1016/j.ceramint.2023.07.175
64. U.G. Issever, G. Kilic, E. Ilik, The Impact of CuO on physical, structural, optical and thermal properties of dark VPB semiconducting glasses. Opt. Mater. (Amst.) **116**, 111084 (2021). https://doi.org/10.1016/j.optmat.2021.111084
65. S. Qian, L. Huang, S. Zhao, S. Xu, Luminescent properties of Tb^{3+} doped high density borogermanate scintillating glasses. J. Rare Earths **35**(8), 787–790 (2017). https://doi.org/10.1016/S1002-0721(17)60977-3
66. M. Kumar, A.S. Rao, Influence of Tb^{3+} ions concentration and temperature on lithium bismuth alumino borosilicate glasses for green photonic device applications. Opt. Mater. (Amst.) (2021). https://doi.org/10.1016/j.optmat.2021.111439
67. W. Chewpraditkul, Y. Shen, D. Chen, A. Beitlerova, M. Nikl, Luminescence of Tb^{3+}-doped high silica glass under UV and X-ray excitation. Opt. Mater. (Amst.) **35**(3), 426–430 (2013). https://doi.org/10.1016/j.optmat.2012.09.012
68. D. Umamaheswari, B.C. Jamalaiah, T. Sasikala, T. Chengaiah, I.G. Kim, L. Rama Moorthy, Photoluminescence and decay behavior of Tb^{3+} ions in sodium fluoro-borate glasses for display devices. J. Lumin. **132**(5), 1166–1170 (2012). https://doi.org/10.1016/j.jlumin.2011.12.080
69. A.J. Silversmith, D.M. Boye, K.S. Brewer, C.E. Gillespie, Y. Lu, D.L. Campbell, 5D3→7FJ emission in terbium-doped sol-gel glasses. J. Lumin. **121**(1), 14–20 (2006). https://doi.org/10.1016/j.jlumin.2005.09.009
70. P. Nachimuthu, R. Jagannathan, Tb3+ fluorescence as a probe of cluster formation in lead oxyfluoride glasses. J. Non Cryst. Solids **183**(1–2), 208–211 (1995). https://doi.org/10.1016/0022-3093(94)00586-9
71. C.H. Kam, S. Buddhudu, Luminescence and decay behaviour of Tb_3+:ZrF 4-BaF_2-LaF_3-YF_3-AlF_3-NaF optical glasses. Phys. B Condens. Matter **337**(1–4), 237–244 (2003). https://doi.org/10.1016/S0921-4526(03)00409-5
72. H.C. Lu, J.I. Lo, Y.C. Peng, S.L. Chou, B.M. Cheng, W.H. Hung, Far-UV photoluminescence of boron-doped diamond: cross interaction between boron and diamond. Carbon N. Y. **134**, 448–451 (2018). https://doi.org/10.1016/j.carbon.2018.04.017
73. H.C. Lu, Y.C. Peng, M.Y. Lin, S.L. Chou, J.I. Lo, B.M. Cheng, Analysis of boron in diamond with UV photoluminescence. Carbon N. Y. **111**, 835–838 (2017). https://doi.org/10.1016/j.carbon.2016.10.082
74. A.T. Collins, The characterisation of point defects in diamond by luminescence spectroscopy. Diam. Relat. Mater. **1**(5–6), 457–469 (1992). https://doi.org/10.1016/0925-9635(92)90146-F
75. J.A. Freitas, K. Doverspike, P.B. Klein, Y.L. Khong, A.T. Collins, Luminescence studies of nitrogen- and boron-doped diamond films. Diam. Relat. Mater. **3**(4–6), 821–824 (1994). https://doi.org/10.1016/0925-9635(94)90277-1
76. S. Hemalatha, M. Nagaraja, A. Madhu, K. Suresh, N. Srinatha, Spectroscopic studies of transition metal ion-doped borate glasses for optical applications. Mater. Today Proc. **49**, 1875–1879 (2021). https://doi.org/10.1016/j.matpr.2021.08.075